Cloaking via heating: Approach to acoustic cloaking of an actuated boundary in a rarefied gas

A. Manela and L. Pogorelyuk

Citation: Physics of Fluids (1994-present) **26**, 062003 (2014); doi: 10.1063/1.4884369
View online: http://dx.doi.org/10.1063/1.4884369
View Table of Contents: http://scitation.aip.org/content/aip/journal/pof2/26/6?ver=pdfcov
Published by the AIP Publishing

PHYSICS OF FLUIDS **26**, 062003 (2014)

Cloaking via heating: Approach to acoustic cloaking of an actuated boundary in a rarefied gas

A. Manela[a] and L. Pogorelyuk
Faculty of Aerospace Engineering, Technion – Israel Institute of Technology, Haifa 32000, Israel

(Received 12 April 2014; accepted 5 June 2014; published online 24 June 2014)

Existing studies on sound wave propagation in rarefied gases examine sound generation by actuated boundaries subject to isothermal boundary conditions. While these conditions are simple to analyze theoretically, they are more challenging to apply in practice compared to heat-flux conditions. To study the effect of modifying the thermal boundary conditions, the present work investigates the impact of replacing the isothermal with heat-flux conditions on propagation of acoustic waves in a microchannel. The linearized problem is formulated for an ideal hard-sphere gas, and the effect of heat-flux prescription is demonstrated through comparison with counterpart results for isothermal boundaries. Analytical solutions are obtained for a gas at collisionless (highly rarefied) and continuum-limit conditions, and validated through comparison with direct simulation Mote Carlo predictions. Remarkably, it is found that prescription of heat flux at the walls, altering the energy balance within the medium, has a significant effect on acoustic wave propagation in the gas. In particular, when optimized with respect to the boundary acoustic signal applied, the heat flux condition may be used to achieve "acoustic cloaking" of the moving wall, a much desired property in classical acoustics. © *2014 AIP Publishing LLC*. [http://dx.doi.org/10.1063/1.4884369]

I. INTRODUCTION

Acoustic cloaking,[1] the concept of making a structure "acoustically invisible" at given flow conditions, has recently become a key objective in various disciplines in classical acoustics, ranging from aeroacoustics to underwater acoustics, and spanning over the entire range of audible sound frequencies. Making use of the theory of transformation acoustics,[2,3] existing studies have applied a coordinate-transformation-based technique to show that sound scattering from a given body can be arbitrarily controlled through optimized manipulation of structure material and surrounding medium parameters. A variety of mechanical and electromechanical means have been suggested to monitor sound-wave propagation, leading to growing use in metamaterials and metafluids to achieve acoustic sound reduction (e.g., Refs. 4 and 5).

While acoustic cloaking has been widely studied in the context of continuum fluid mechanics, no counterpart research has been taking place in the field of non-continuum flows. Yet, apart from the fundamental interest in studying cloaking at non-continuum conditions, such investigation may be helpful in shedding light on cloaking at continuum-limit conditions, as well as relate macroscopic mechanisms of noise control to microscopic-level phenomena. It therefore appears worthwhile to investigate cloaking methodologies in the context of rarefied gas flows, encountered in cases where the characteristic macroscopic length and time scales of the acoustic setup are of the order of, or smaller than, the mean free path and mean free time of a gas molecule, respectively.

Propagation of sound waves in rarefied gases has been studied in a large number of works, beginning in the middle of the 20th century and evolving through to current research.[6–17] Owing to

[a]Author to whom correspondence should be addressed. Electronic mail: amanela@technion.ac.il

the relative complexity of non-continuum flows, most studies have focused on a fundamental setup of an infinite planar wall undergoing small-amplitude periodic oscillations in the normal direction, and investigated the sound generated at semi-infinite and finite flow domains. Other works have followed to consider the case of sound generation by non-periodic boundary animation.[18,19] While the acoustic pressure field has been investigated in detail in all of these studies, no attempt has been made to develop means for monitoring the outcome sound. In addition, common to all mentioned works is the prescription of *isothermal* conditions on the confining walls. Inevitably, to maintain constant wall temperature, time-dependent non-zero heat flux must occur at the boundaries. This, in turn, affects the energy balance within the gas and resulting flow field.

While isothermal-wall conditions are relatively simple to analyze, they are challenging to follow in practice. Thus, in a typical experiment, it would be preferable to monitor the heat flux at a boundary rather than its temperature. When doing so, the wall temperature becomes an *a priori* unknown variable, consequence of the interaction between the gas and the wall. From the theoretical point of view, this complicates the formulation of the problem. Yet, from the practical point of view, this may enable control over the properties of the generated sound, as will be discussed below.

In parallel with studies on propagation of acoustic waves in rarefied gases, a set of works have appeared which consider the gas response to *thermoacoustic* excitation, in the form of temperature variation of its boundaries (see Refs. 20–24 and works cited therein). Similar to mechanical actuation, temperature variations result in generation of pressure waves, which propagate with velocity equal to the acoustic wave velocity. In a single work where both acoustic and thermoacoustic effects were considered, Kalempa and Sharipov[25] have studied the combined effects of harmonically varying both normal boundary velocity and temperature in time. To the extent that walls temperature is "prescribed," this set of studies, including Ref. 25, can be considered similar to the above acoustic-wave investigations. Here, as before, an *a priori* unknown amount of heat flux must be supplied to the walls to maintain them at the required temperature.

The purpose of the present contribution is to investigate the effect of replacing the isothermal boundary conditions with heat-flux conditions on propagation of sound waves in a microchannel.[26] Apart from the fundamental interest in such an investigation, the analysis may be of practical importance, as it is much easier to monitor heat-flux at a boundary than to control its temperature. Moreover, we suggest the heat-flux prescribed at a boundary to be used as a "control parameter," to affect the properties of wall-motion acoustic radiation; specifically, it will be demonstrated that an optimal choice of the heat-flux profile may lead to effective cloaking of the moving boundary, in a mechanism named "thermal cloaking."

The paper outline is as follows. In Sec. II, the general problem of acoustic wave propagation in a microchannel is described. Limit-case analytical solutions (at collisionless and continuum-limit conditions) are derived, and description of the direct simulation Monte Carlo (DSMC scheme), used for numerical solution, is provided. Numerical and analytical results are presented in Sec. III, demonstrating the effect of heat-flux boundary conditions on sound wave propagation. Concluding comments are given in Sec. IV.

II. PROBLEM FORMULATION

Consider a perfect monatomic gas layer of uniform density ρ_0^* confined between two parallel infinitely long diffusely reflecting walls placed at $x^* = \mp L^*/2$ (with asterisks denoting dimensional quantities). The gas is initially at rest and in thermodynamic equilibrium with the boundaries, which, at time $t^* < 0$, maintain the temperature T_0^*. At time $t^* \geq 0$, one or both walls move in the normal direction into the gas layer according to a prescribed (arbitrary) small-amplitude velocity profile,

$$\varepsilon \mathbf{U}_{w_\pm}^*(t^*) = \varepsilon U_{w_\pm}^*(t^*)\hat{\mathbf{x}}, \tag{1}$$

with "plus" and "minus" signs corresponding to the motion of walls located at $x^* = -L^*/2$ and $x^* = +L^*/2$, respectively. Simultaneously, heat-flux at the walls is prescribed by

$$\varepsilon \mathbf{Q}_{w_\pm}^*(t^*) = \varepsilon Q_{w_\pm}^*(t^*)\hat{\mathbf{x}}. \tag{2}$$

The temperature of both boundaries is left unprescribed for $t^* \geq 0$, and is determined through the interaction between the walls and the gas. In both (1) and (2), it is assumed that $\varepsilon \ll 1$, so that the system description may be linearized about its initial equilibrium.

To render the problem dimensionless, we normalize position, velocity, and time by L^*, $U^*_{th} = \sqrt{2R^*T^*_0}$ (marking the mean thermal speed of gas molecules, with R^* denoting the specific gas constant), and acoustic time-scale $t^*_a = L^*/U^*_{th}$, respectively. Density and temperature are scaled by ρ^*_0 and T^*_0, respectively, and the heat flux is normalized by $\rho^*_0 U^{*3}_{th}$. The resulting non-dimensional problem is governed by the scaled profiles of boundaries motion and heat-flux injection, as well as by the Knudsen number,

$$Kn = l^*/L^*, \tag{3}$$

marking the ratio between the mean free path of a gas molecule l^* and the channel width L^*. The physical problem will be analyzed in the entire range of Knudsen numbers: the limit-cases of highly rarefied (collisionless) and near-continuum conditions are considered in Secs. II A and II B, respectively; description of the direct simulation Monte Carlo method, to be used to solve the problem at arbitrary Knudsen numbers, is given is Sec. II C.

A. Ballistic-flow limit

In the framework of kinetic theory of gases, the gas state is described by the velocity distribution function,

$$f(x, t, \mathbf{c}) = F[1 + \varepsilon\phi(x, t, \mathbf{c})], \tag{4}$$

wherein $\mathbf{c} = (c_x, c_y, c_z)$ is the vector of molecular velocity, and $F = \pi^{-3/2}\exp[-c^2]$ is the equilibrium Maxwellian distribution. Assuming the Knudsen number, defined in Eq. (3), to be infinitely large, we neglect the effect of molecular collisions and consider the collisionless Boltzmann equation for $\phi(\mathbf{x}, t, \mathbf{c})$,

$$\frac{\partial\phi}{\partial t} + c_x\frac{\partial\phi}{\partial x} = 0. \tag{5}$$

The equation is supplemented by an initial condition,

$$\phi(x, t = 0^-, \mathbf{c}) = 0, \tag{6}$$

together with a linearized form of the diffuse boundary condition imposed at the walls,[27]

$$\phi(x = \mp 1/2, t, c_x \gtrless 0) = \rho_\pm(t) + 2c_x U_{w_\pm}(t) + T_{w_\pm}(t)(c^2 - 3/2). \tag{7}$$

In (7), $U_{w_\pm}(t)$ are obtained from the scaled form of (1). Notably, $\rho_\pm(t)$ and $T_{w_\pm}(t)$ are yet to be determined, with $T_{w_\pm}(t)$ marking the scaled time-variation of walls temperature perturbation.

Taking the Laplace transform of (5) and making use of (6) and (7) yield the solution

$$\hat{\phi}(s, x, c_x \gtrless 0, c_y, c_z) = \left[\hat{\rho}_\pm(s) + 2c_x\hat{U}_{w_\pm}(s) + \hat{T}_{w_\pm}(s)\left(c^2 - \frac{3}{2}\right)\right]\exp\left[-\frac{s}{c_x}\left(x \pm \frac{1}{2}\right)\right], \tag{8}$$

where s is the Laplace variable and $\hat{}$ denotes the Laplace transform of a function. By inversion of (8) we obtain

$$\phi(t, x, c_x \gtrless 0, c_y, c_z) = \rho_\pm(t_\pm) + 2c_x U_{w_\pm}(t_\pm) + T_{w_\pm}(t_\pm)(c^2 - 3/2), \tag{9}$$

where $t_\pm = t - (x \pm 1/2)/c_x$. The fields $\rho_\pm(t)$ and $T_{w_\pm}(t)$ are determined by imposing macroscopic no-penetration conditions,

$$\frac{1}{\pi^{3/2}}\int_{-\infty}^{\infty} c_x\phi\left(x = \mp\frac{1}{2}\right)\exp(-c^2)\mathrm{d}\mathbf{c} = U_{w_\pm}(t), \tag{10}$$

and heat-flux conditions,

$$\frac{1}{2\pi^{3/2}}\int_{-\infty}^{\infty} c^2 c_x\phi\left(x = \mp\frac{1}{2}\right)\exp(-c^2)\mathrm{d}\mathbf{c} - \frac{5}{4}U_{w_\pm}(t) = Q_{w_\pm}(t), \tag{11}$$

at the walls.[27] Substituting (9) into (10) and (11), and carrying out appropriate changes of variables, lead to a set of coupled integral equations, imposing no-penetration,

$$\rho_{\pm}(t)+\frac{1}{2}T_{w_{\pm}}(t)-2\int_0^t\frac{\rho_{\mp}(\tau)}{(t-\tau)^3}\exp\left[-\frac{1}{(t-\tau)^2}\right]d\tau-\int_0^t\frac{T_{w_{\mp}}(\tau)}{(t-\tau)^3}\left[\frac{2}{(t-\tau)^2}-1\right]\exp\left[-\frac{1}{(t-\tau)^2}\right]d\tau=\pm\sqrt{\pi}U_{w_{\pm}}(t)\mp4\int_0^t\frac{U_{w_{\mp}}(\tau)}{(t-\tau)^4}\exp\left[-\frac{1}{(t-\tau)^2}\right]d\tau, \tag{12}$$

and heat flux,

$$\rho_{\pm}(t)+\frac{3}{2}T_{w_{\pm}}(t)-\int_0^t\frac{\rho_{\mp}(\tau)}{(t-\tau)^3}\left[\frac{1}{(t-\tau)^2}+1\right]\exp\left[-\frac{1}{(t-\tau)^2}\right]d\tau-\int_0^t\frac{T_{w_{\mp}}(\tau)}{(t-\tau)^3}\left[\frac{1}{(t-\tau)^4}+\frac{1}{2(t-\tau)^2}+\frac{1}{2}\right]\exp\left[-\frac{1}{(t-\tau)^2}\right]d\tau=\pm\frac{5}{4}\sqrt{\pi}U_{w_{\pm}}(t)\pm2\sqrt{\pi}Q_{w_{\pm}}(t)\mp2\int_0^t\frac{U_{w_{\mp}}(\tau)}{(t-\tau)^4}\left[\frac{2}{(t-\tau)^2}-1\right]\exp\left[-\frac{1}{(t-\tau)^2}\right]d\tau, \tag{13}$$

at the walls. The equations should be solved in conjunction with the initial conditions

$$\rho_{\pm}(0)=\pm(7\sqrt{\pi}/8)U_{w_{\pm}}(0)\mp\sqrt{\pi}Q_{w_{\pm}}(0)\quad\text{and}\quad T_{\pm}(0)=\pm(\sqrt{\pi}/4)U_{w_{\pm}}(0)\pm2\sqrt{\pi}Q_{w_{\pm}}(0). \tag{14}$$

The initial-value problem is solved numerically, for given choices of $U_{w_{\pm}}(t)$ and $Q_{w_{\pm}}(t)$, using an Euler-type method. Once solutions for $\rho_{\pm}$ and $T_{w_{\pm}}$ are obtained, the probability density function perturbation ϕ in (9) is known, and the $O(\varepsilon)$ perturbations of all hydrodynamic fields are computed through appropriate quadratures over the molecular velocity space.[27]

B. Continuum limit

To analyze the limit of small Knudsen numbers, we make use of a continuum model, based on the continuum (Navier-Stokes-Fourier) equations, supplemented by impermeability and heat-flux conditions at the boundaries. The model is similar to the continuum-limit scheme applied in previous analyses (e.g., Ref. 19), yet is repeated here for completeness and to emphasize on the differences in boundary conditions.

Starting with the set of unsteady one-dimensional continuum equations (non-dimensionalized using the scales introduced in the beginning of Sec. II), and linearizing about the initial equilibrium state, we obtain balances of mass, momentum, and energy for the $O(\varepsilon)$ density, normal velocity, and temperature perturbations,

$$\frac{\partial\rho}{\partial t}+\frac{\partial u}{\partial x}=0\,, \tag{15}$$

$$\frac{\partial u}{\partial t}=-\frac{1}{2}\left(\frac{\partial\rho}{\partial x}+\frac{\partial T}{\partial x}\right)+\frac{4\widetilde{Kn}}{3}\frac{\partial^2u}{\partial x^2}\,, \tag{16}$$

and

$$\frac{\partial T}{\partial t}=\frac{\gamma\widetilde{Kn}}{Pr}\frac{\partial^2T}{\partial x^2}-(\gamma-1)\frac{\partial u}{\partial x}\,. \tag{17}$$

Here, $\widetilde{Kn}=\nu^*/U_{th}^*L^*$ is the modified Knudsen number, with ν^* denoting the mean kinematic viscosity of the gas. The modified Knudsen number is related to Kn through

$$\widetilde{Kn}=\frac{\nu^*}{U_{th}^*l^*}Kn, \tag{18}$$

where $\nu^*/U_{th}^* l^* = 5\sqrt{\pi}/16$ for a hard-sphere gas model, to be considered hereafter.[28] In Eq. (17), γ and Pr mark the ratio of specific heats and Prandtl number, respectively, with $\gamma = 5/3$ and $Pr = 2/3$ for a hard-sphere gas. Equations (15)-(17) are supplemented by the boundary conditions

$$u = U_{w_\pm}(t) \text{ and } \frac{15\widetilde{Kn}}{8}\frac{\partial T}{\partial x} = Q_{w_\pm}(t) \text{ at } x = \mp 1/2, \tag{19}$$

imposing impermeability, and specifying the magnitude of heat flux at the walls. Note that, in accordance with the continuum Fourier law of heat conduction, the heat flux in (19) is proportional to the temperature gradient at the boundary. By applying this condition, the continuum description is fully adopted, with no specific prescription of "temperature jump" at the boundaries. This is in difference from standard formulations of continuum-limit models (e.g., Ref. 19), where isothermal boundaries are considered.[28] The effect of gas rarefaction in the present formulation is tacitly inserted through the value of $\widetilde{Kn}$ in the momentum and energy balances (see (16) and (17)). As will be demonstrated in Sec. III, this model is found adequate to capture the system behavior at small (yet non-zero) Knudsen numbers.

The problem is solved by applying time Fourier transform to Eqs. (15)-(19). This yields a system of ordinary equations in the frequency ω-domain,

$$\mathrm{i}\omega\bar{\rho} + \bar{u}' = 0 \ , \ \mathrm{i}\omega\bar{u} = -\frac{1}{2}\left(\bar{\rho}' + \bar{T}'\right) + \frac{4\widetilde{Kn}}{3}\bar{u}'' \text{ and } \mathrm{i}\omega\bar{T} = \frac{5\widetilde{Kn}}{2}\bar{T}'' - \frac{2}{3}\bar{u}' \ , \tag{20}$$

where bars indicate Fourier-transformed fields, together with boundary conditions

$$\bar{u} = \bar{U}_{w_\pm}(\omega) \text{ and } \frac{15\widetilde{Kn}}{8}\bar{T}' = Q_{w_\pm}(t) \text{ at } x = \mp 1/2, \tag{21}$$

in which primes denote differentiations with x. The density and velocity perturbations can be eliminated using

$$\bar{\rho} = \frac{\mathrm{i}}{\omega}\bar{u}' \ , \ \bar{u} = -\frac{15\widetilde{Kn}}{4\omega}\left(\frac{1}{2\omega} + \frac{4\mathrm{i}\widetilde{Kn}}{3}\right)\bar{T}''' - \left(2\widetilde{Kn} - \frac{5\mathrm{i}}{4\omega}\right)\bar{T}' \tag{22}$$

to yield a single equation for the temperature,

$$\frac{5\widetilde{Kn}}{2}\left(\frac{4\widetilde{Kn}}{3} - \frac{\mathrm{i}}{2\omega}\right)\bar{T}'''' - \frac{1}{6}\left(23\mathrm{i}\omega\widetilde{Kn} + 5\right)\bar{T}'' - \omega^2\bar{T} = 0, \tag{23}$$

solved in conjunction with the four boundary conditions

$$-\frac{15\widetilde{Kn}}{4\omega}\left(\frac{1}{2\omega} + \frac{4\mathrm{i}\widetilde{Kn}}{3}\right)\bar{T}''' - \left(2\widetilde{Kn} - \frac{5\mathrm{i}}{4\omega}\right)\bar{T}' = \bar{U}_\pm(\omega) \quad \text{and}$$

$$\frac{15\widetilde{Kn}}{8}\bar{T}' = Q_{w_\pm}(t) \text{ at } x = \mp 1/2\,. \tag{24}$$

The characteristic polynomial of Eq. (23) has four distinct roots,

$$r_{1,2}(\omega) = \pm\left[\frac{-a_1 + \sqrt{a_1^2 - 4a_2a_0}}{2a_2}\right]^{1/2} \quad \text{and} \quad r_{3,4}(\omega) = \pm\left[\frac{-a_1 - \sqrt{a_1^2 - 4a_2a_0}}{2a_2}\right]^{1/2}, \tag{25}$$

where a_0, a_1, and a_2 are the coefficients multiplying $\bar{T}$, $\bar{T}''$, and $\bar{T}''''$ in (23), respectively. The solution for the temperature perturbation is given by

$$\bar{T}(x,\omega) = \sum_{k=1}^{4} C_k(\omega)\exp\left[r_k(\omega)x\right], \tag{26}$$

where the constants C_k are determined using the boundary conditions (24). Expressions for the Fourier-transformed density and velocity perturbations then follow from substitution of Eq. (26) into Eq. (22). The time-domain solution is obtained by taking the real part of the inverse Fourier transform of each of the transformed hydrodynamic fields.

C. DSMC scheme

The prevalent numerical scheme for analyzing rarefied gas flows is a stochastic particle method, known as the DSMC method.[29] The method simulates the trajectories of a large number of molecules, taking account of both collisions between molecules and molecular-boundary reflections, at discrete time intervals. Making use of a hard-sphere model of molecular interaction, the present work applies a one-dimensional version of the DSMC scheme, to simulate the gas response to acoustic and thermal excitations generated by fully diffuse boundaries. Results for isothermal-boundary domain, presented in Sec. III, have been generated for reference via the standard approach described in Ref. 29. Prescribing heat flux conditions on the boundaries has required usage of a closed-loop controller for the temperature of the boundaries. Towards this end, consider the total normalized energy E_k transferred between the particles and a given boundary at the time interval $0 \le t \le t_k$. Given the heat flux $q(t)$ prescribed at that wall, we define the energy transfer error function,

$$\tilde{E}_k = \int_0^{t_k} q(\tau)\, d\tau - E_k, \tag{27}$$

and apply a discrete proportional-integral controller,

$$T_{k+1} = 1 + K_p \tilde{E}_k + K_i \sum_{j=0}^{k} \tilde{E}_j. \tag{28}$$

Here, T_{k+1} is the normalized temperature of the wall at time-step $k+1$, and K_p and K_i denote proportional and integral gains, respectively. A positive $\tilde{E}_k$ corresponds to a case where the energy transferred by the wall to the incoming particles is lower than required by the prescribed boundary condition. In this case, the K_p proportional gain term increases the temperature to compensate for the outcome error. At the same time, the K_i accumulation term is present to eliminate the steady-sate error in the temperature, $\tilde{E}_k(t \to \infty)$, which otherwise should have been present to allow for non-zero steady state temperature perturbation, $T_k(t \to \infty) - 1 \neq 0$ (see Eqs. (31) and (32)). Both gain values are chosen ≈ 0.1 in all cases, as larger values cause undesired effects such as negative temperature, in the presence of simulation noise.

For consistency with our linearized setup, the amplitude of boundary excitation was chosen small such that the maximum velocity in the channel does not surpass 2% of the mean thermal velocity. Typically, the small perturbations relative to the noise level inherent in Monte Carlo simulations greatly diminish the signal-to-noise ratio of the results. In this respect, a low-variance direct Monte Carlo (LVDSMC) scheme may have been more suitable to reduce the statistical noise.[30,31] Nevertheless, the present choice of standard DSMC method has been made due to three main reasons: first, the relative simplicity of DSMC algorithm; second, the availability of powerful computational resources; and third, to demonstrate that the common DSMC algorithm is able to produce results that are of sufficient quality. In terms of analysis, the main purpose of the numerical method applied is to support the analytical findings. In this context, the close agreement found between DSMC and analytical results (see Sec. III) justifies application of the conventional Monte Carlo algorithm.

To achieve the desired precision of the numerical solution, we have used spatial discretization of 100 cells across the channel with 200 sub-cells each, and time discretization of 10^4 steps per run, lasting several ballistic time scales. The number of cells and sub-cells was chosen so that further refinement of the grid did not cause noticeable changes in the results. Each run consisted of approximately 10^9 particles simulated on 24 Intel Xeon E5645 cores for 24 h.

III. RESULTS

The analysis described in Sec. II can be applied to study the gas response to any prescribed small-amplitude motion and heat-flux at the boundaries. To demonstrate our findings, we consider a case where the boundary at $x = -0.5$ is excited via velocity and heat "bump-like" excitations of

identical durations,

$$U_{w_+}(t) = \begin{cases} 1 & , \quad 0 \le t \le t_b \\ 0 & , \quad \text{otherwise} \end{cases}, \quad Q_{w_+}(t) = \begin{cases} Q_0 & , \quad 0 \le t \le t_b \\ 0 & , \quad \text{otherwise} \end{cases}, \tag{29}$$

where t_b governs the bumps duration and is taken $t_b = 0.1$ (in ballistic time units, L^*/U^*_{th}), to consider "short-time" excitation. This choice facilitates production of DSMC results, as the system equilibration time is short enough to require relatively short simulation times. The wall at $x = 0.5$ is taken stationary ($U_{w_-} = 0$) and adiabatic ($Q_{w_-} = 0$). We start by studying the gas response to bump actuation in a thermally insulated channel ($Q_0 = 0$), and compare our findings with counterpart results for a gas confined between isothermal walls.[19] We then turn to consider a non-adiabatic setup, where non-zero heat-flux bump is applied at $x_0 = -0.5$, and study its effect on outcome radiation. We skip a detailed study of the breakdown of the limit-case analytical solutions with varying Kn, as a similar study has been conducted in Ref. 19 in the context of the isothermal problem. Instead, we focus on examining the extreme cases of large and small Knudsen numbers. Qualitatively similar findings to those presented below (not presented here for brevity) have been obtained using DSMC calculations at intermediate ($0.1 < Kn < 1$) Knudsen numbers.

A. Adiabatic channel

Figures 1 and 2 present time variations of the velocity, temperature, and pressure perturbations, obtained in the adiabatic and isothermal cases, for $Kn = 10$ (Fig. 1) and $Kn = 0.01$ (Fig. 2), at a fixed location $x = -0.4$ across the gap. Each figure shows comparison between analytical

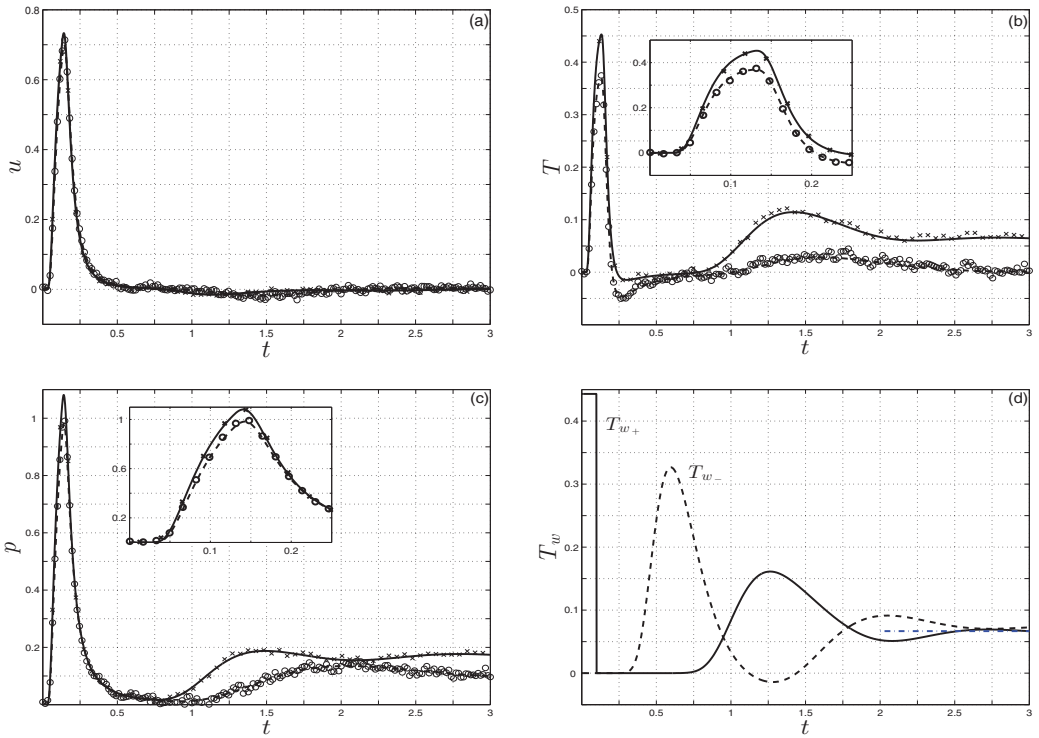

FIG. 1. Effect of adiabatic boundary conditions on the response of a gas at $Kn = 10$ to bump actuation: (a)-(c) Time-variations of velocity (Fig. 1(a)), temperature (Fig. 1(b)), and pressure (Fig. 1(c)) perturbations at $x = -0.4$. Solid and dashed lines mark analytical results for collisionless gas confined between adiabatic (Eq. (29) with $Q_0 = 0$) and isothermal[19] boundaries, respectively. Crosses and circles show counterpart DSMC data for hard-sphere gas at $Kn = 10$. Insets in Figs. 1(b) and 1(c) show zoom into the time interval of initial wavefront passage. (d) Time-variation of adiabatic walls temperature, T_{w_+} (solid line) and T_{w_-} (dashed line), obtained from the analytical collisionless solution. Short dashed-dotted line marks steady-state equilibrium value, achieved at long times (see (31)).

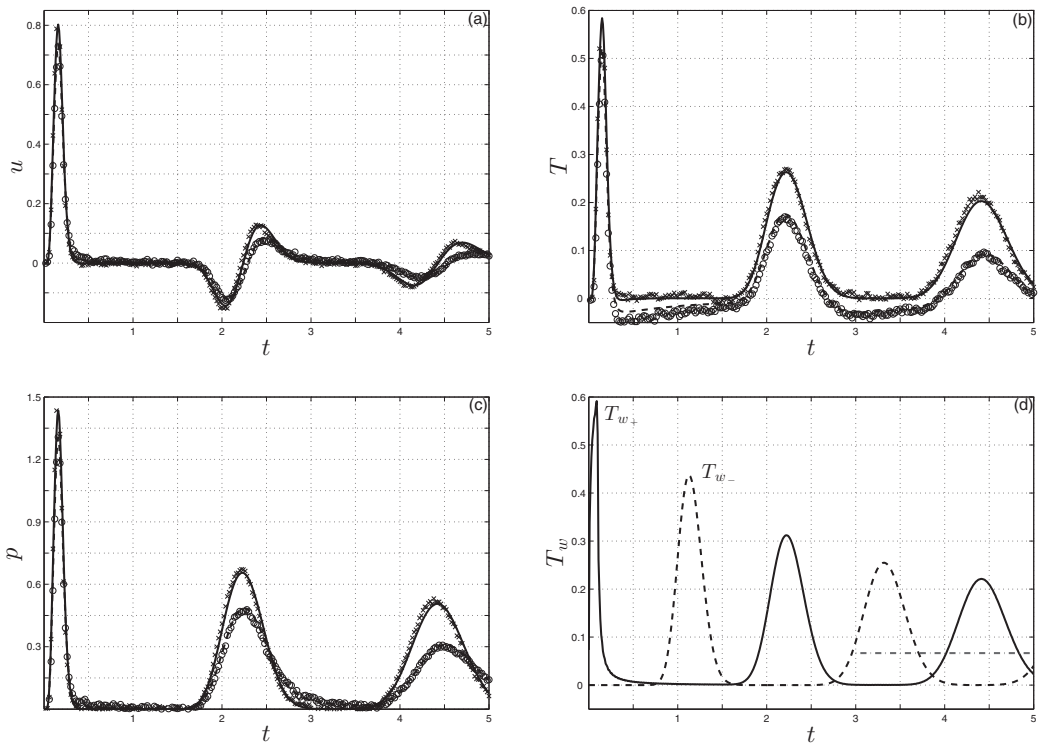

FIG. 2. Effect of adiabatic boundary conditions on the response of a gas at $Kn = 0.01$ to bump actuation: (a)-(c) Time-variations of velocity (Fig. 1(a)), temperature (Fig. 1(b)), and pressure (Fig. 1(c)) perturbations at $x = -0.4$. Solid and dashed lines mark analytical results for hard-sphere gas confined between adiabatic (Eq. (29) with $Q_0 = 0$) and isothermal[19] boundaries, respectively. Crosses and circles show counterpart DSMC data. (d) Time-variation of adiabatic walls temperature, T_{w_+} (solid line) and T_{w_-} (dashed line), obtained from the analytical continuum-limit solution. Short dashed-dotted line marks steady-state equilibrium value, achieved at long times (see (31)).

(ballistic-limit solution in Fig. 1; continuum-limit solution in Fig. 2) and numerical DSMC solutions. The analytical results in the isothermal-boundaries setup are obtained using the scheme detailed in Ref. 19. Figs. 1(d) and 2(d) show time variations of adiabatic walls temperature perturbations at $Kn = 10$ and $Kn = 0.01$, respectively. Given the vastly different methods of calculation, and the inevitable statistical noise inherent in DSMC results (see Sec. II C), we find the close agreement between all sets of results satisfactory. This supports application of the analytical schemes, presented in Sec. II, to analyze the system response at the specified large and small Knudsen numbers.

Starting with the large-Kn case in Fig. 1, we observe several common features between the adiabatic- and isothermal-boundary setups. Thus, at early times there exists an initial time interval, during which all perturbations equal zero in both isothermal and adiabatic cases (see the insets in Figs. 1(b) and 1(c) at early times). This "retarded time" interval reflects the time it takes the moving-wall signal to reach the point in space where perturbations are measured. As the signal wavefront passes a point in space, all hydrodynamic perturbations exhibit sharp variations in their values. With increasing time, the mutual effects of both walls are reflected at each point in the gas domain. At late times, the gas approaches its new equilibrium state through a series of decaying waves propagating across the gap.

While the above general features are common to both isothermal and adiabatic setups, other properties are distinct. To start with, the first sharp maximum observed in each of the thermodynamic perturbations (temperature and pressure) is larger in the adiabatic setup than in the isothermal case (see the insets in Figs. 1(b) and 1(c)). Physically, maintaining the boundary at a constant temperature, while moving it into the gas layer, requires heat to be removed from the system. This is achieved through active "cooling," or outgoing heat-flux, occurring at the boundary. System internal energy is consequently reduced, resulting in lowering the amplitudes of signal wavefronts. In the adiabatic

case, no heat flux is allowed at the walls, and thus the gas is comparably "heated" in the vicinity of the moving boundary. This, in turn, results in relative enforcement of the generated pressure wave. The heating effect is also reflected by an initial rise in the temperature of the moving boundary T_{w_+} (which is maintained fixed in the isothermal setup), as depicted by the solid line in Fig. 1(d).

The different thermal conditions also result in a difference in the final equilibrium state achieved by the system. For the case of an isothermal wall displaced a t_b-distance into the gas domain (in εL^* units) after the bump, the new equilibrium state (with vanishing velocity field) is given by

$$\rho_{\text{iso}}(t \to \infty) = t_b \quad , \quad T_{\text{iso}}(t \to \infty) = 0 \quad , \quad p_{\text{iso}}(t \to \infty) = t_b. \tag{30}$$

In difference from Eq. (30), when the system is adiabatic, a non-zero change occurs in the walls temperature owing to their displacement (see Fig. 1(d)), which determines the gas temperature in equilibrium. Using thermodynamic considerations for an ideal gas undergoing adiabatic compression, this change can be determined. Adding it to the steady-state density perturbation common to both adiabatic and isothermal setups, the adiabatic equilibrium state is given by

$$\rho_{\text{ad}}(t \to \infty) = t_b \quad , \quad T_{\text{ad}}(t \to \infty) = 2t_b/3 \quad , \quad p_{\text{ad}}(t \to \infty) = 5t_b/3. \tag{31}$$

These steady-state values are clearly recovered in the late-time behavior in Fig. 1. It is this very effect of heat-flux removal at the boundaries, resulting in reduced temperature and pressure levels in the isothermal case, that will be applied later on to reduce the acoustic pressure in the system and achieve "cloaking" in a non-adiabatic setup (see Sec. III B). The new equilibrium state is achieved after $t \approx 2$, which corresponds to approximately one-fifth of the mean free time for the present choice of $Kn = 10$. Given the relatively short relaxation process, it is indeed expected that the collisionless analysis should predict the exact numerical solution well.

Traversing to the low-Kn case presented in Fig. 2, several qualitative differences are observed between the system behavior at collisionless and continuum-limit conditions. These are common to both adiabatic and isothermal setups. The most visible difference is in the oscillatory behavior of the system at small Kn, being much weaker at high-Kn flow conditions. This is accompanied by extension in equilibration time with decreasing Kn, being $t \gtrsim 15$ (outside the time interval presented in the figure) for $Kn = 0.01$. As observed and rationalized in Ref. 19, we find that the Knudsen number, governing the amount of collisions experienced by a molecule while passing through the channel, can be viewed as a "damping coefficient" of the acoustic response, in both types of thermal boundary conditions.

Comparing between the isothermal- and adiabatic-setup responses in Fig. 2, the differences obtained are similar to those found in the high-Kn case of Fig. 1: that is, owing to the lack of a "cooling mechanism" in the adiabatic system, the acoustic wave is characterized by higher wavefront amplitudes, accompanied by higher steady-state pressure levels. The steady-state values, not visible in Fig. 2 owing to the short time interval presented (see the equilibrium temperature value marked by the dashed-dotted line in Fig. 2(d)), are identical to those predicted by Eqs. (30) and (31).

B. Non-adiabatic channel

The results in Figs. 1 and 2 indicate that the propagation of acoustic pressure within the channel is affected by the thermal boundary condition applied, with the pressure perturbation being larger in the adiabatic compared to the isothermal case. While the total effect may appear small in the results of Figs. 1(c) and 2(c) (being a difference of only few percents between the setups in the peak pressure), it appears worthwhile to examine the impact of varying the heat flux at the actuated wall on sound propagation. We therefore reapply excitation (29) to the system, now with $Q_0 \neq 0$ as a "control" parameter, governing the amount of heat added ($Q_0 > 0$) or removed ($Q_0 < 0$) at the actuated boundary. The boundary at $x = 0.5$ is kept stationary and adiabatic in all cases, as noted in the beginning of Sec. III.

Figure 3 studies the effect of heat-flux parameter Q_0 on the system pressure perturbation in both collisionless (Fig. 3(a)) and continuum-limit ($Kn = 0.01$, Fig. 3(b)) conditions. The solid lines and crosses mark adiabatic-channel ($Q_0 = 0$) results (analytic and DSMC, respectively), identical with the solid lines and crosses in Figs. 1(c) and 2(c). The dashed and dashed-dotted lines, together with

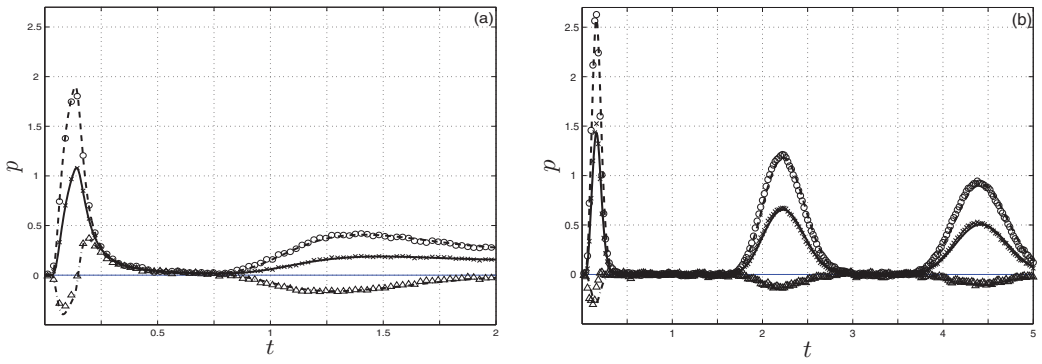

FIG. 3. Effect of boundary heat-flux condition on the acoustic pressure obtained at $x = -0.4$ at $Kn = 10$ (Fig. 3(a)) and $Kn = 0.01$ (Fig. 3(b)) conditions. Solid, dashed, and dashed-dotted lines mark analytical results for adiabatic ($Q_0 = 0$), "boundary heating" ($Q_0 = 1$), and "boundary cooling" ($Q_0 = -1.5$) conditions. Crosses, circles, and triangles present respective DSMC predictions. Thin blue lines mark lines of zero acoustic pressure, for reference.

circles and triangles, show counterpart analytic and DSMC results for $Q_0 = 1$ ("boundary heating") and $Q_0 = -1.5$ ("boundary cooling") conditions. Again we note the close agreement between two sets of data, in support of accurateness of both schemes of solution.

Observing the results in Fig. 3, and in agreement with the discussion of Figs. 1 and 2, we find that boundary heating ($Q_0 > 0$) yields an increase in the system pressure level: the added heat superposes with the pressure signal generated by boundary motion, and strengthens the outcome pressure wave. However, applying outgoing heat-flux at the boundaries ($Q_0 < 0$) has the counter effect on sound wave propagation, acting to cancel out the pressure wave generated by the moving boundary. The extent to which the latter reduces the adiabatic signal is remarkable, in both collisionless and continuum-limit conditions, resulting in a vanishingly small pressure signal, common to the entire channel (see Fig. 5). Physically, the mechanism through which boundary heat-flux affects the acoustic field can now be rationalized: boundary heating, similar to wall animation, results in generation of a thermoacoustic pressure wave, propagating in a velocity equal to the velocity of the actuated-boundary acoustic disturbance. When opposite in phase (as in the case of boundary cooling applied to a boundary moving into the gas; see the dashed-dotted lines and triangles in Fig. 3), the thermoacoustic disturbance tends to reduce the acoustic wave. The effectiveness of this "cloaking" mechanism may be optimized using the heat-flux parameter Q_0, as demonstrated below.

Making use of Eq. (31) for the steady state in an adiabatic channel, and superposing the effect of heat flux addition at an animated boundary through an energy balance, the values of steady-state perturbations at non-adiabatic conditions corresponding to excitation (29) may be obtained,

$$\rho_{Q_0}(t \to \infty) = t_b \ , \ T_{Q_0}(t \to \infty) = \frac{2t_b}{3}(1 + 2Q_0) \ , \ p_{Q_0}(t \to \infty) = \frac{t_b}{3}(5 + 4Q_0). \tag{32}$$

It has been verified that these values are recovered at long times by our calculations. Notably, Eq. (32) indicates that thermal heating effectively cancels out the long-time acoustic pressure when $Q_0 = -5/4$. At this value of Q_0, the final temperature perturbation is negative ($T_{Q_0} \approx -0.1$), indicating that steady-state cloaking is accompanied by overall cooling of the gas (see Fig. 6).

To gain further insight into the effect of heat-flux parameter on the system acoustic response, we consider the impact of Q_0 on the entire equilibration process of the system, beginning at the initial time of excitation. Towards this end, we define the *total integrated* pressure and temperature perturbations,

$$\Pi(t_f) = \int_0^{t_f} \int_{-0.5}^{0.5} |p(x,t)| \, \mathrm{d}x\mathrm{d}t \quad \text{and} \quad \Theta(t_f) = \int_0^{t_f} \int_{-0.5}^{0.5} |T(x,t)| \, \mathrm{d}x\mathrm{d}t, \tag{33}$$

respectively, measuring the total pressure and temperature disturbances occurring across the gap at times $0 \le t \le t_f$. The upper time limit t_f is chosen arbitrarily, yet our calculations indicate that the results presented below remain qualitatively similar for different choices of t_f. While the optimal

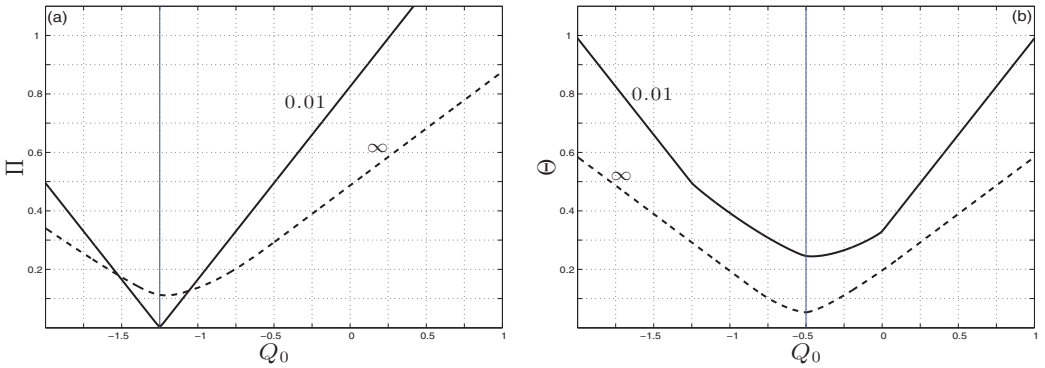

FIG. 4. Variation of total integrated pressure (Fig. 4(a)) and temperature (Fig. 4(b)) perturbations (see (33)) with heat-flux parameter Q_0 at the indicated values of $Kn = 0.01$ (with $t_f = 5$) and $Kn \to \infty$ (with $t_f = 3$). Results are based on collisionless and continuum-limit analytical solutions. Vertical lines mark values of Q_0 for which steady-state acoustic pressure ($Q_0 = -5/4$, Fig. 4(a)) and temperature perturbation ($Q_0 = -1/2$, Fig. 4(b)) vanish (see (32)).

value of $Q_0 = -5/4$ for achieving long-time cloaking of the system is obvious from (32), the purpose of the remaining discussion is to study the effect of heat-flux parameter on the *transient* behavior of the system. We therefore choose values of t_f for which the system has not yet, or just reached, equilibrium.

Following the definitions in Eq. (33), Figure 4 presents the variations of integrated pressure and temperature with heat-flux parameter Q_0 at continuum-limit ($Kn = 0.01$) and collisionless ($Kn \to \infty$) flow conditions. Having confirmed in Figs. 1–3 that our limit-case solutions agree well with DSMC predictions, the results presented hereafter are based on analytic solutions only. For the calculation of $\Pi(t_f)$ and $\Theta(t_f)$, values of $t_f = 5$ and $t_f = 3$ were taken for $Kn = 0.01$ and $Kn \to \infty$, respectively. Focusing on Fig. 4(a), we find that the conditions for "transient cloaking" coincide with "steady-state cloaking": that is, the choice $Q_0 = -5/4$ results in the smallest value for Π, for both large and small values of Kn. The cloaking effect is most remarkable at the small-Kn case, where pressure fluctuations practically vanish in both time and space (see Fig. 5). As visible in Fig. 4(b), optimized acoustic cloaking is accompanied by an increase in the integrated temperature perturbation compared to the adiabatic case (cf. the values of Θ at $Q_0 = -5/4$ and $Q_0 = 0$ for both Knudsen numbers). It is therefore the transfer between acoustic and thermal energies which enables the reduction of acoustic pressure with varying Q_0. Interestingly, Fig. 4(b) indicates that the optimized reduction in gas temperature perturbation is obtained, for both Kn, at $Q_0 = -1/2$. This result coincides with the value of Q_0 required for long-time vanishing of T_{Q_0}, according to Eq. (32).

To complement the discussion in Fig. 4, Figs. 5 and 6 present time-space maps of gas acoustic pressure (Fig. 5) and temperature perturbation (Fig. 6) at both large ($Kn \to \infty$) and small ($Kn = 0.01$) Knudsen numbers. Fig. 5 shows comparison between the acoustic pressure at adiabatic ($Q_0 = 0$, Figs. 5(a) and 5(c)) and "optimized cloaking" ($Q_0 = -5/4$, Figs. 5(b) and 5(d)) conditions. Fig. 6 shows respective time-space temperature maps at $Q_0 = -5/4$. To facilitate comparison between adiabatic and non-adiabatic cases, all parts in Fig. 5 are presented using the same color-bar scale.

Starting with the adiabatic-system response in Figs. 5(a) and 5(c), one can easily trace the acoustic wave propagation across the channel, initiated at $t = 0$ at $x = -0.5$, and undergoing a series of wall reflections with gradually decaying amplitude at later times. The decay rate is markedly faster in the collisionless case, as also noted in the discussion of Figs. 1 and 2. Comparing between the adiabatic-setup results and their non-adiabatic $Q_0 = -5/4$ counterparts in Figs. 5(b) and 5(d), the overall cloaking effect is evident. The effect is most remarkable in the $Kn = 0.01$ case shown in Fig. 5(d): as supported by the minimum value of Π in the solid line in Fig. 4(a), the thermoacoustic wave in this setup essentially cancels out the acoustic disturbance, resulting in a vanishingly small pressure perturbation even at the initial time of boundary animation. The thermodynamic charac-

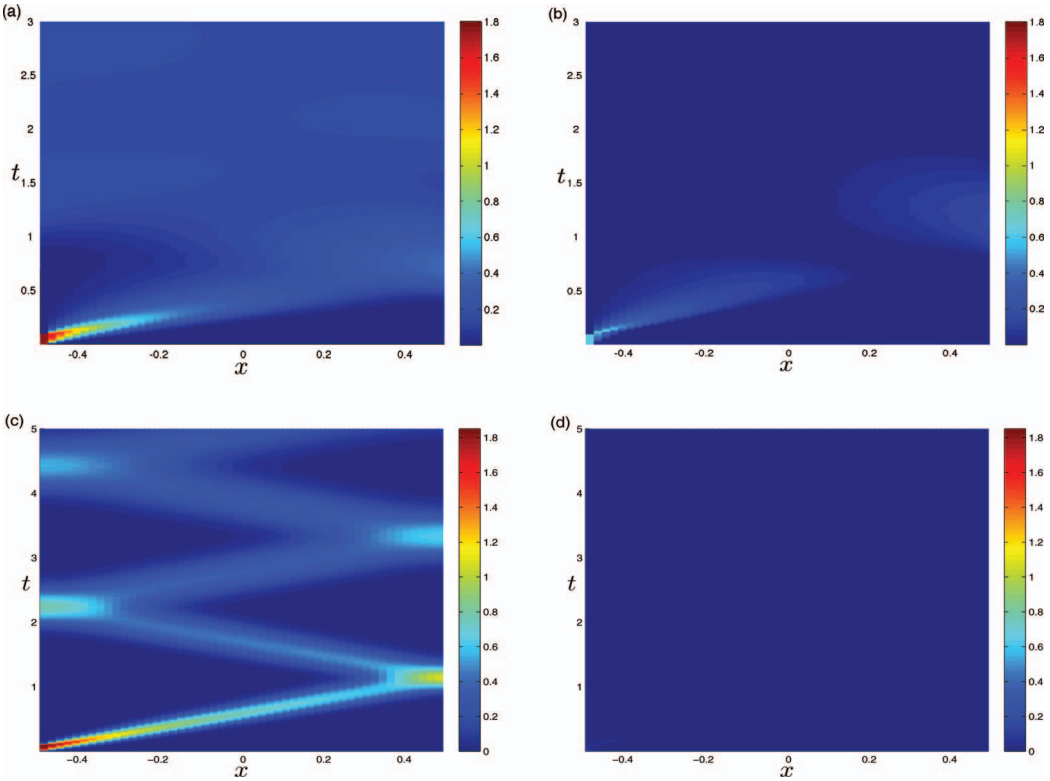

FIG. 5. Time-space maps of system acoustic pressure excited by boundary bump actuation: (a) and (b) collisionless gas with adiabatic ($Q_0 = 0$, Fig. 5(a)) and "cooled" ($Q_0 = -5/4$, Fig. 5(b)) boundary; (c) and (d) $Kn = 0.01$ gas with adiabatic ($Q_0 = 0$, Fig. 5(c)) and "cooled" ($Q_0 = -5/4$, Fig. 5(d)) boundary. Results are based on collisionless and continuum-limit analytical solutions.

terization of the non-adiabatic setup is completed in Fig. 6, indicating the accompanying transfer between acoustic and thermal energies within the gas. As noted in Fig. 5(b), the cloaking of sound is accompanied by overall cooling of the gas. Interestingly, the wave-structure of the propagation of temperature disturbance, visible in the adiabatic case (that is, in the temperature counterparts of Figs. 5(a) and 5(c), not presented here for brevity), is much less observed in the non-adiabatic map, indicating that the thermoacoustic disturbance at these conditions acts to smoothen temperature gradients within the medium.

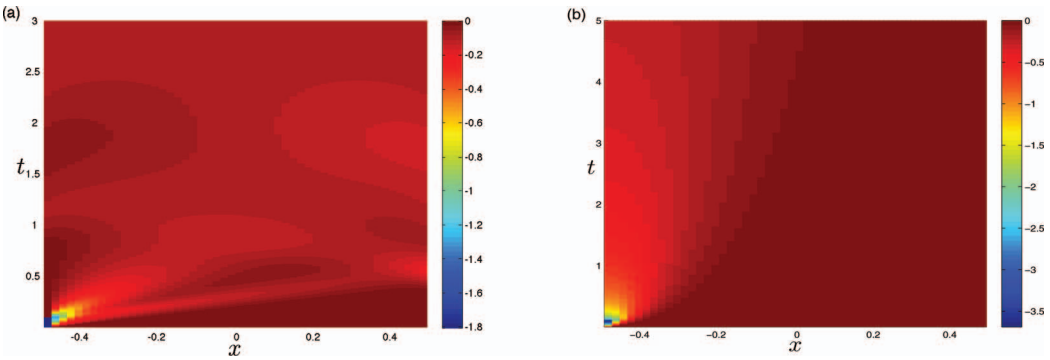

FIG. 6. Time-space maps of gas temperature perturbation excited by actuated non-adiabatic boundary with $Q_0 = -5/4$: (a) collisionless gas; (b) $Kn = 0.01$ gas. Results are based on collisionless and continuum-limit analytical solutions.

IV. CONCLUSION

We have studied the acoustic effect of replacing the isothermal conditions on a boundary, commonly used in acoustic-wave analyses of rarefied and continuum gas flows, with heat-flux conditions. The problem was formulated and solved for an ideal hard-sphere gas undergoing purely diffuse reflections with the channel walls, and the effect of heat-flux insulation was demonstrated through comparison with results obtained for a channel with isothermal walls. Considering non-adiabatic setup, it was demonstrated that significant reduction in the motion-generated acoustic disturbance can be achieved through optimized prescription of heat flux at the wall. The result was supported by steady-state thermodynamic considerations, indicating that the "cloaking" effect is inevitably accompanied by an appropriate change in the gas temperature, through transfer between acoustic and thermal energies.

The problem was solved analytically, in limit cases of large (collisionless) and small (continuum-limit) Knudsen-number conditions, and results were found in close agreement with numerical DSMC predictions. While the conventional DSMC method may not be the most efficient numerical tool to be used in the present linearized setup (compared to, say, more sophisticated low-variance Monte Carlo schemes[30,31]), we have applied it here due to its relative simplicity, and to demonstrate its ability to produce results that are of sufficient quality, in support of our analytical findings. In doing so, the present contribution primarily aims at demonstrating the mechanism of thermal cloaking through our closed-form solutions, in which results could be easily obtained. A detailed study of the breakdown of the limit-case solutions with varying Kn was not presented, as a similar investigation (leading to qualitatively similar conclusions) can be found in the isothermal-boundary problem studied in Ref. 19. In essence, our numerical results for intermediate values of the Knudsen number show similar trends, in terms of the effect of boundary heating, to those presented in the two limit cases.

Our findings are presented for a single test-case of bump-like boundary animation, specified by $U_{w_+}(t)$ in Eq. (29). Yet, our scheme can be readily applied to consider the gas response to any small-amplitude boundary excitation, for both wall motion and thermal heating profiles. As mentioned in the beginning of Sec. III, the present choice facilitates production of DSMC results, as the system equilibration time is short enough to require only short simulation times. Apart from studying other excitation profiles, it would be of practical interest to study the system response in a semi-infinite setup, where only the actuating boundary is present. In such a case, continuum conditions should prevail soon after the initiation of boundary excitation (once sufficient time has elapsed since initial perturbation), and the efficiency of the thermal cloaking mechanism may be tested. Such an investigation is part of a study currently in progress.

While application of thermal heating to achieve acoustic cloaking appears new in the present context, recent studies on the thermal properties of metamaterials have suggested thermal monitoring as means for obtaining wave cloaking in various other disciplines. These include, among others, studies on optical cloaking (making objects "invisible" through heating[32,33]) and electromagnetic wave formation.[34] In this respect, the present contribution may be considered as a demonstration of the impact of heating on the acoustic properties of a mechanically actuated boundary immersed in a gas. Future studies are required to investigate the practical feasibility (in terms of heat-exchange requirements) of the proposed mechanism for controlling the sound in finite domains, and to consider the heat-flux effect on sound propagation in fluids other than ideal gases.

[1] A. N. Norris, "Acoustic cloaking theory," Proc. R. Soc. A **464**, 2411–2434 (2008).
[2] H. Chen and C. T. Chan, "Acoustic cloaking in three dimensions using acoustic metamaterials," Appl. Phys. Lett. **91**, 183518 (2007).
[3] S. A. Cummer and D. Schurig, "One path to acoustic cloaking," New J. Phys. **9**, 45–51 (2007).
[4] A. N. Norris, "Acoustic metafluids," J. Acoust. Soc. Am. **125**, 839–849 (2009).
[5] B.-I. Popa, L. Zigoneanu, and S. A. Cummer, "Experimental acoustic ground cloak in air," Phys. Rev. Lett. **106**, 253901 (2011).
[6] M. Greenspan, "Propagation of sound in five monatomic gases," J. Acoust. Soc. Am. **28**, 644–648 (1956).
[7] E. Meyer and G. Sessler, "Schallausbreitung in Gasen bei hohen Frequenzen und sehr niedrigen Drucken," Z. Phys. **149**, 15–29 (1957).
[8] L. Sirovich and J. K. Thurber, "Propagation of forced sound waves in rarefied gas dynamics," J. Acoust. Soc. Am. **37**, 329–339 (1965).

[9] G. Maidanik, H. L. Fox, and M. Heckl, "Propagation and reflection of sound in rarefied gases. I. Theoretical," Phys. Fluids **8**, 259–265 (1965).
[10] J. Foch and G. E. Uhlenbeck, "Propagation of sound in monatomic gases," Phys. Rev. Lett. **19**, 1025–1027 (1967).
[11] S. K. Loyalka and T. C. Cheng, "Sound-wave propagation in a rarefied gas," Phys. Fluids **22**, 830–836 (1979).
[12] S. Stefanov, P. Gospodinov, and C. Cercignani, "Monte Carlo simulation and Navier-Stokes finite difference calculation of unsteady-state rarefied gas flows," Phys. Fluids **10**, 289–300 (1998).
[13] N. G. Hadjiconstantinou, "Sound wave propagation in transition-regime micro- and nanochannels," Phys. Fluids **14**, 802–809 (2002).
[14] F. Sharipov, W. Marques, Jr., and G. M. Kremer, "Free molecular sound propagation," J. Acoust. Soc. Am. **112**, 395–401 (2002).
[15] F. Sharipov and D. Kalempa, "Numerical modeling of the sound propagation through a rarefied gas in a semi-infinite space on the basis of linearized kinetic equation," J. Acoust. Soc. Am. **124**, 1993–2001 (2008).
[16] D. Kalempa and F. Sharipov, "Sound propagation through a rarefied gas confined between source and receptor at arbitrary Knudsen number and sound frequency," Phys. Fluids **21**, 103601 (2009).
[17] H. Struchtrup, "Resonance in rarefied gases," Contin. Mech. Thermodyn. **24**, 361–376 (2012).
[18] T. Tsuji and K. Aoki, "Moving boundary problems for a rarefied gas: Spatially one-dimensional case," J. Comput. Phys. **250**, 574–600 (2013).
[19] A. Manela, G. A. Radtke, and L. Pogorelyuk, "On the damping effect of gas rarefaction on propagation of acoustic waves in a microchannel," Phys. Fluids **26**, 032001 (2014).
[20] A. Manela and N. G. Hadjiconstantinou, "On the motion induced in a gas confined in a small-scale gap due to instantaneous boundary heating," J. Fluid Mech. **593**, 453–462 (2007).
[21] A. Manela and N. G. Hadjiconstantinou, "Gas motion induced by unsteady boundary heating in a small-scale slab," Phys. Fluids **20**, 117104 (2008).
[22] A. Manela and N. G. Hadjiconstantinou, "Gas-flow animation by unsteady heating in a microchannel," Phys. Fluids **22**, 062001 (2010).
[23] T. Doi, "Numerical analysis of the time-dependent energy and momentum transfers in a rarefied gas between two parallel planes based on the linearized Boltzmann equation," J. Heat Transfer ASME **133**, 022404 (2010).
[24] M. Vargas, S. Stefanov, and V. Roussinov, "Transient heat transfer flow through a binary gaseous mixture confined between coaxial cylinders," Int. J. Heat Mass Transfer **59**, 302–315 (2013).
[25] D. Kalempa and F. Sharipov, "Sound propagation through a rarefied gas: Influence of the gas-surface interaction," Int. J. Heat Fluid Flow **38**, 190–199 (2012).
[26] Hereafter, the term "microchannel" corresponds to a one-dimensional slab where only normal-to-wall flow velocity exists with no parallel-to-wall velocity.
[27] M. N. Kogan, *Rarefied Gas Dynamics* (Plenum, New York, 1969).
[28] Y. Sone, *Molecular Gas Dynamics: Theory, Techniques, and Applications* (Birkhäuser, Boston, 2007).
[29] G. Bird, *Molecular Gas Dynamics and the Direct Simulation of Gas Flows* (Clarendon, Oxford, 1994).
[30] T. M. M. Homolle and N. G. Hadjiconstantinou, "A low-variance deviational simulation Monte Carlo for the Boltzmann equation," J. Comput. Phys. **226**, 2341–2358 (2007).
[31] G. A. Radtke, N. G. Hadjiconstantinou, and W. Wagner, "Low-noise Monte Carlo simulation of the variable hard-sphere gas," Phys. Fluids **23**, 030606 (2011).
[32] S. Guenneau, C. Amra, and D. Veynante, "Transformation thermodynamics: Cloaking and concentrating heat flux," Opt. Express **20**, 8207–8218 (2012).
[33] M. Wegener, "Metamaterials beyond optics," Science **342**, 939–940 (2013).
[34] M. Kadic, T. Buckmann, R. Schittny, and M. Wegener, "Metamaterials beyond electromagnetism," Rep. Prog. Phys. **76**, 126501 (2013).